Determination of the dominant factors of hydrogen embrittlement in austenitic stainless steel
オーステナイト系ステンレス鋼における水素脆化支配因子の決定

Principal Investigator: Chiba University, Graduate School of Engineering,
Assistant Professor Luca Chiari
研究代表者　千葉大学大学院工学研究院　助教　キアリ　ルカ

1. Introduction

Although the utilization of hydrogen as a clean energy vector to meet the needs of a more environmentally friendly society is getting full-fledged, hydrogen embrittlement in metals poses a significant problem for its widespread application. Hydrogen embrittlement is a reduction in the mechanical properties of a large class of susceptible metals, such as their decrease in ductility and early fracture, when they are used in a hydrogen environment. Several theories of hydrogen embrittlement have been developed and consistent supporting experimental evidence has been accrued over the years [1]. Notwithstanding this large research effort in attempting to understand the embrittlement process, the underlying mechanisms are still not completely understood.

Amongst the proposed hydrogen-embrittlement mechanisms, the hydrogen-enhanced strain-induced vacancy formation (HESIV) model argues that the atomic vacancies formed by dislocation cutting upon tensile testing are stabilized by bonding with hydrogen, which in turn promotes their aggregation by forming vacancy clusters and induces the destabilization of the plastic deformation [2]. In fact, theoretical calculations show that hydrogen reduces the vacancy formation energy in γ-iron by 0.23 eV [3]. Hence, the experimental elucidation at the atomic level of the interaction between hydrogen, vacancies and dislocation motion is very important to detect the dominant defects in hydrogen embrittlement. For this purpose, a non-invasive and highly sensitive analysis of lattice defects is required.

Positron annihilation lifetime spectroscopy (PALS) is a non-destructive technique used to detect vacancy-type defects, such as dislocations, atomic vacancies, and vacancy clusters, with a high sensitivity of up to 10^{-7} in atomic ratio, from measurements of the positron lifetime in the material [4]. The application of PALS to hydrogen embrittlement studies revealed so far that stretching susceptible metals in the presence of hydrogen promoted the formation of vacancy clusters. However, the formation of vacancy clusters is promoted in α-iron (bcc phase) even in the presence of hydrogen under stretching conditions that do not lead to hydrogen embrittlement (e.g. fast strain rate). Therefore,

vacancy clusters were ruled out as the primary defects responsible for hydrogen embrittlement. In α-iron, the hydrogen diffusion coefficient at room temperature is very large and, therefore, the hydrogen-charged samples were quenched in liquid nitrogen immediately after stretching, and PALS measurements were carried out at variable temperatures. Those results have shown that, under the conditions where hydrogen embrittlement occurred, mobile monovacancies were detected in the range between 250 K to 420 K, whereas already grown vacancy clusters had formed when hydrogen embrittlement did not occur. Therefore, it was concluded that hydrogen binds to and stabilizes monovacancies by forming vacancy-hydrogen complexes, which are the primary controlling factor of hydrogen embrittlement in α-iron. Those defects accumulate locally on the slip surface due to the dislocation motion and become the starting point of cracks.

In austenitic stainless steel SUS 304, which is a γ-phase (fcc phase), it is believed that hydrogen embrittlement depends on the γ-phase stability, as the phase transformation to the processing-induced α' martensite phase and stacking faults are closely related to hydrogen [5]. However, the formation of vacancy clusters was observed at a strain value at which no processing-induced α' martensitic transformation occurred. Therefore, hydrogen embrittlement in the austenitic stainless steel phase cannot be explained only by the formation of the processing-induced martensite phase, and it is necessary to consider the hydrogen embrittlement process of the γ-phase itself. One of the possible causes of hydrogen embrittlement may be that hydrogen-induced vacancies aggregate in a high-strain region such as the boundary between the γ-phase and the ε phase (hcp) to form vacancy clusters and serve as a starting point for fracture [6]. Preliminary PALS measurements in SUS 304 pointed out that the vacancy-hydrogen complexes diffuse into the steel already at the initial stage of elongation.

In order to elucidate the hydrogen embrittlement behaviour in austenitic stainless steels, it is necessary to examine the vacancy generation process, and a non-destructive and highly sensitive analysis is required. In this research, the formation process of hydrogen-induced vacancies in austenitic stainless steel SUS 304 after exposure to a hydrogen environment was investigated. *In-situ* analysis of the defect formation behaviour at the boundary between the elastic region and the plastic deformation region during tensile testing was carried out by PALS measurements.

2. Experimental methods

2.1 Sample preparation

All the samples were manufactured from austenitic stainless steel SUS 304 thin plates. The chemical composition of the present steel SUS 304 is shown in Table 1 and matches

that specified by the Japanese Industrial Standards.

Table 1　Chemical composition of the present SUS 304 samples

C	Si	Mn	P	S	Ni	Cr	Fe
<0.03	<1.00	<2.00	<0.045	<0.03	8.00~10.50	18.00~20.00	balance

The SUS 304 thin plates were processed into dumbbell-shaped specimens for use in tensile testing by electric discharge machining. Fig. 1 shows a schematic diagram of the sample shape and size. The specimen width is 10 mm, gauge length is 20 mm, and thickness is 0.2 mm. A notch is provided at the center of the gauge section to concentrate the tensile stress in that area.

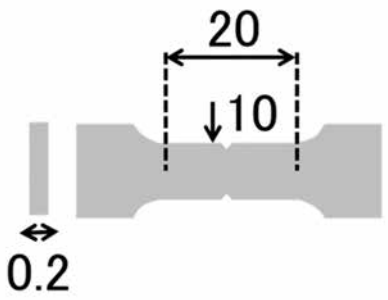

Fig. 1　Schematic diagram of the sample shape and size Units: mm

The samples underwent solution treatment to remove the defects generated during the rolling and processing of the material. The solution treatment was performed in an Ar atmosphere using an infrared gold image furnace. The solution treatment temperature was 900°C, the heating time was 4 h (heating rate 4°C/min), and the holding time was 5 min. Thereafter, the sample was left to cool down to room temperature. As the samples showed a black oxide film of several μm in thickness after the solution treatment, their surface layer was removed by mechanical and chemical polishing.

2.2 Hydrogen charging

Hydrogen was introduced into the samples by the electrolytic hydrogen charging method. A 3% NaCl + 3 g/l NH_4SCN aqueous solution was used as the electrolyte. The charging time was 48 hours at a current density of 50 A/m^2.

2.3 Tensile tests

After hydrogen charging, the samples were subject to tensile testing. The strain rate was 2.75×10^{-5}/s for the samples strained up to fracture, whereas the strain rate was 4.17×10^{-3}/s for the samples strained up to strain values of 5%. For the latter samples, the measurements were carried out *in situ* on the sample maintained stretched at the same strain value for the whole duration of the measurement.

2.4 PALS measurements

Positron annihilation lifetime spectroscopy is a non-destructive technique used to detect open-volume defects in a variety of materials with high sensitivity. PALS can determine the type, size and relative concentration of vacancy-type defects based on the positron lifetime in the material, i.e. the time from the positron injection into the sample to the annihilation with an electron of the material. The positron source is made of ^{22}Na sealed within Kapton films from which high-energy positrons are generated by β^+ decay and can penetrate into metals up to about 100 μm in depth before annihilation. The γ-rays produced by the positron generation (start signal) and the positron annihilation (stop signal) are detected by two photomultiplier tubes coupled to BaF_2 scintillators. The output signals are recorded and processed by a digital storage oscilloscope. Each positron lifetime spectrum was obtained by integrating at least one million counts and at least three spectra were collected for each sample to achieve enough statistical accuracy. The present PALS measurements were carried out *in situ* while keeping the samples stretched at a given strain value.

Fig. 2 shows a typical lifetime spectrum of stainless steel SUS 304 and its decomposition into various components. The spectrum is analysed by fitting the data with the sum of exponential decay functions using least squares regression. The number of fitting components corresponds to the number of defect types in which positrons annihilated. Typically, the lifetime components correspond to positron annihilation in the bulk (lifetime value of around 110 ps), at dislocations and/or monovacancies (~160-180 ps), and in vacancy clusters (~200-400 ps).

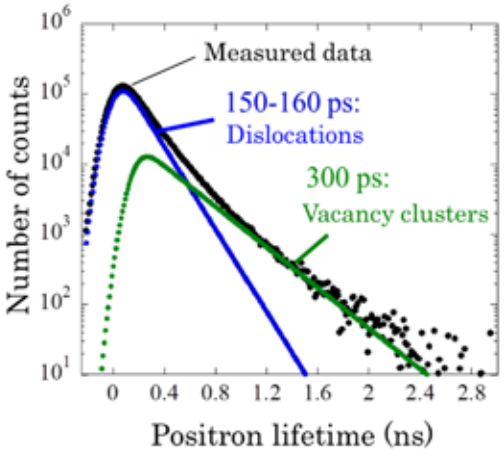

Fig. 2　Typical positron lifetime spectrum for hydrogen-charged and fractured stainless steel SUS 304 and spectrum decomposition into two lifetime components

The vacancy size can be quantitatively obtained from measurements of the positron lifetime value by comparing with first-principle calculations which correlate defect size and positron lifetime (Fig. 3). The relative concentration of each defect type in the sample is proportional to the relative intensity of the respective lifetime component.

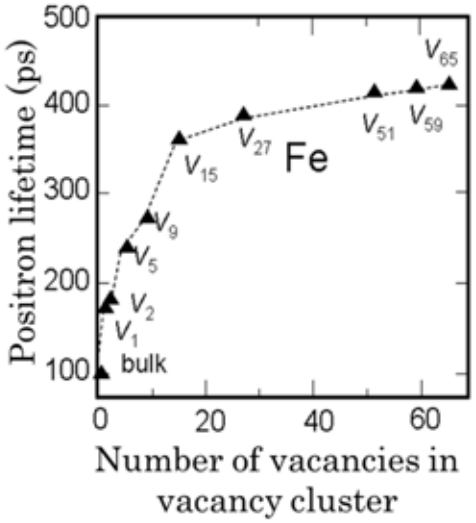

Fig. 3　First-principle calculation correlating the positron lifetime value to the number of atomic vacancies in a vacancy cluster in α-iron [7].

3. Results and discussion

First of all, the effect of the hydrogenation on the mechanical properties of the SUS 304 samples was investigated by tensile testing. Fig. 4 shows the results of the tensile tests on the hydrogen-free and hydrogen-charged samples. The sample subject to hydrogen charging is clearly hydrogen embrittled, as its strain value at fracture and its maximum stress value are significantly reduced with respect to the non-hydrogenated sample. However, the stress-strain curves of the two samples are not significantly different to each other in the elastic region.

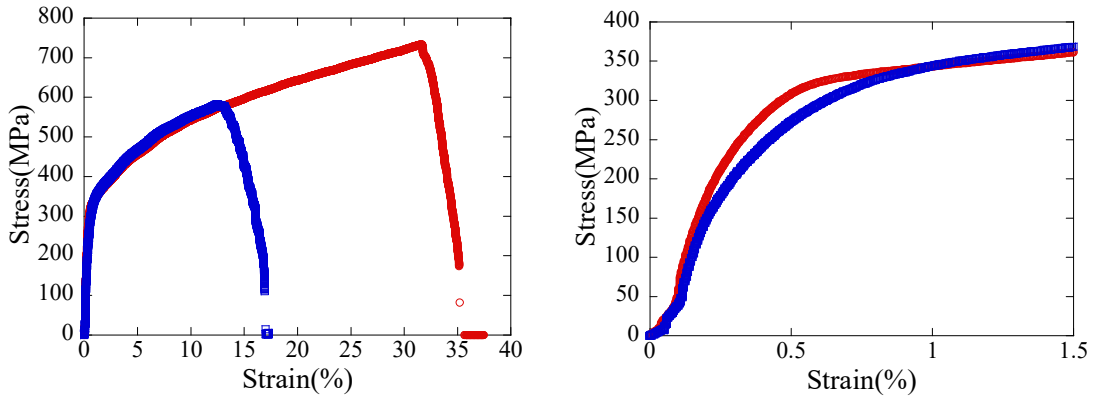

Fig. 4 Left: stress-strain curves of the hydrogen-free (red) and hydrogen-charged (blue) samples. Right: expanded view of the elastic region.

Fig. 5 shows the positron lifetimes of the hydrogen-free and hydrogen-charged samples before the tensile test. Both samples show a single lifetime of about 110 ps, which corresponds to the known lifetime value for positrons annihilating in the bulk. Since only the bulk component appeared in the hydrogen-charged sample, it is clear that no defects responsible for hydrogen embrittlement had formed during the hydrogen charging stage. Therefore, the hydrogen addition itself is not the cause of the defect generation.

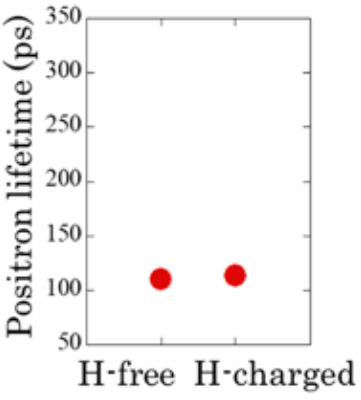

Fig. 5 Positron lifetimes of the hydrogen-free and hydrogen-charged samples

The lifetimes of the hydrogen-free and hydrogen-charged samples after tensile testing until fracture are shown in Fig. 6. In the hydrogen-free fractured sample, a single lifetime of around 165 ps was observed. This value is

consistent with the known lifetimes for positrons annihilating at dislocations and monovacancies. This confirms that dislocations and monovacancies are generated when the sample is subject to tensile deformation. On the other hand, in the hydrogen-charged fractured sample, two lifetime components were observed. The first component was similar in value to that observed in the hydrogen-free fractured sample, thus indicating the formation of dislocations and monovacancies. The second component was significantly longer (285 ps) and can be attributed to positron annihilation at vacancy clusters. Based on the results of the first-principle calculation shown in Fig. 3, we expect these vacancy clusters to be of around 10 atomic vacancies in size. This result shows that vacancy clusters are formed when the hydrogenated sample is stretched and fractured compared to the non-hydrogenated sample. In the tensile tests, a premature fracture was observed in the hydrogenated sample due to the hydrogen embrittlement. Hence, it is concluded that there must be a correlation between the formation of vacancy clusters and the hydrogen embrittlement-related premature fracture.

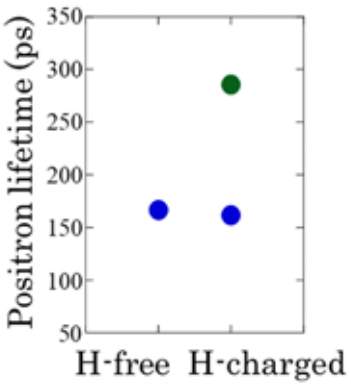

Fig. 6 Positron lifetimes of the hydrogen-free and hydrogen-charged samples after tensile straining until fracture. The blue data correspond to the first component (dislocations and monovacancies), while the green data show the second component (vacancy clusters).

The origin of the relation between the vacancy clusters and the premature fracture can be clarified by studying the defect generation process at the early stage of the tensile deformation. For this purpose, the lifetime was measured at various tensile strain values at the boundary between the elastic region and the plastic deformation region, and compared between the hydrogen-charged and uncharged samples.

First of all, we determined the extent of the elastic region and ensured that the sample condition does not change before and after tensile stretching in the elastic region. For this purpose, PALS measurements were carried out in three stages: before tensile strain is applied (0% strain), while the sample is stretched at a strain value of 0.5%, and after releasing the sample back to its original shape (0% strain because of the elasticity of the sample in this strain region). The measurements were carried out *in situ* while keeping the samples in each condition. Fig. 7 shows the lifetimes measured in these three stages for both the hydrogen-free and hydrogen-charged samples. In both the hydrogen-free and hydrogen-charged samples, only the bulk component of around 110 ps was observed in all three stages. This confirms the elasticity of the sample and that no defects were introduced in the sample upon tensile straining up to this strain value and by hydrogenation. Such measurements were also repeated at a strain value of 1% and the results confirmed the elasticity of the samples up to this strain value and the absence of defects.

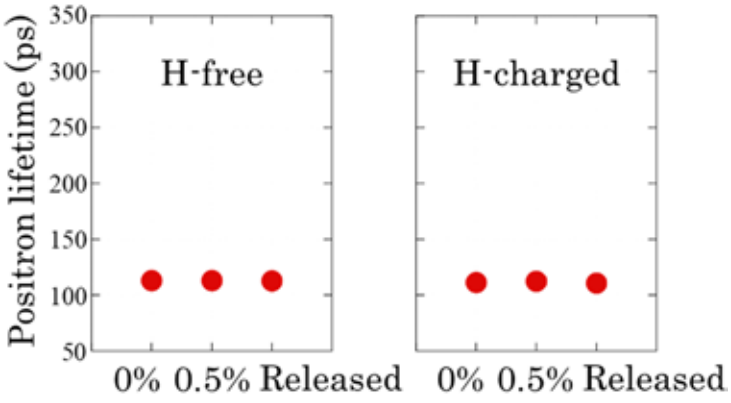

Fig. 7 Positron lifetimes of the hydrogen-free (left) and hydrogen-charged (right) samples before elongation (0%), at a tensile strain of 0.5%, and after release

Next, PALS measurements were carried out at various tensile strain values at the boundary between the elastic region and the initial plastic deformation region to study the defect formation process. The measurements were carried out *in situ* while maintaining the samples in the stretched condition at each strain value. Fig. 8 shows the lifetimes and the intensity of the second component (where present) measured at the strain values of 0%, 0.5% and 1% in the elastic region, and at 3% and 5% in the initial plastic deformation region. The results of the hydrogen-free and hydrogen-charged samples at each strain value are compared. In both the hydrogen-free and hydrogen-charged samples, only one lifetime component corresponding to the bulk was detected up

to the strain value of 1%. This confirms the elastic region and the absence of defects in this range upon tensile testing and hydrogenation. In the hydrogen-free sample, at strain values beyond 1% a second component of 170-180 ps was observed. This defect size is consistent with the generation of dislocations and monovacancies upon the initial plastic deformation of the sample. Although the lifetime of this component did not change by increasing the strain value, its relative intensity doubled when the strain was increased from 3% to 5%. This reflects an increased concentration of dislocations and monovacancies as expected due to the larger tensile strain. On the other hand, in the hydrogen-charged sample a second component of around 250 ps was observed at strain values beyond 1%. This defect size corresponds to that of vacancy clusters composed of ~5 atomic vacancies. As the strain value was increased from 3% to 5%, the relative intensity of this component increased slightly, indicating that their relative concentration also slightly increased. The small change might be due to the fact that the vacancy clusters are not very mobile during room temperature annealing.

The results shown in Fig. 8 resemble those observed in the fractured samples (Fig. 6), in that only dislocations and monovacancies were found in the hydrogen-free sample, whereas vacancy clusters were only detected in the hydrogen-charged sample. Therefore, this corroborates our hypothesis that it is important to study the defect generation process at the boundary between the elastic region and the initial plastic deformation region in order to understand the relation between the formation of vacancy clusters and the hydrogen embrittlement.

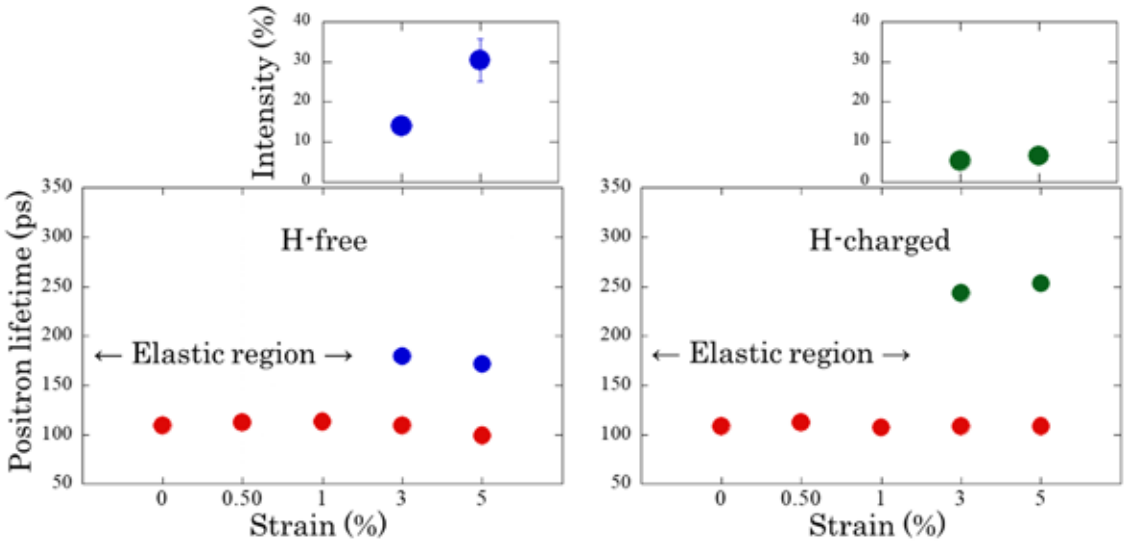

Fig. 8　PALS results for the hydrogen-free (left) and hydrogen-charged (right) samples at various tensile strain values between 0% and 1% in the elastic region, and 3% and 5% in the initial plastic deformation region. Lower panels: positron lifetime of each component; upper panels: relative intensity of the second component. The red data correspond to the bulk component, the blue data to dislocations and monovacancies, and the green data to vacancy clusters.

In terms of the defect formation process and their relevance in the hydrogen embrittlement mechanism, the PALS results of strain-dependence measurements can be interpreted in the following way (see Fig. 9). Upon application of tensile strain, no defects are generated within the elastic region, whereas dislocations and monovacancies are generated as soon as the tensile strain value reaches into the plastic deformation region. In the presence of hydrogen, hydrogen becomes trapped into the monovacancies and stabilizes them by forming vacancy-hydrogen complexes, as suggested by our previous measurements and first-principle calculations. As hydrogen is desorbed by room temperature annealing, the leftover vacancies become mobile and, upon tensile strain, they agglomerate and form vacancy clusters. Through this clustering process, the vacancies become bigger in size but smaller in number, as suggested by the lower intensity of the vacancy cluster component in the hydrogen-charged sample compared to that of the dislocations and monovacancies in the hydrogen-free sample. These vacancy clusters then progressively become bigger in size as the tensile strain increases and eventually become the trigger of the premature fracture.

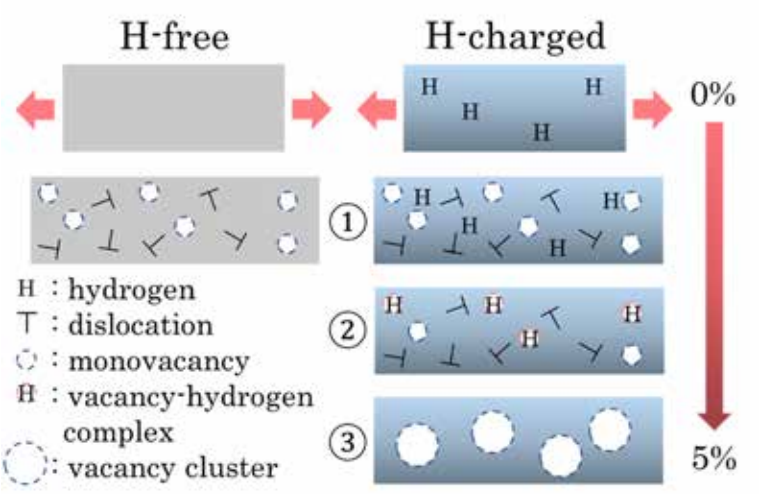

Fig. 9 Schematic diagram of the strain-dependent defect dynamics in the hydrogen-free (left) and hydrogen-charged (right) samples based on the results of Fig. 8: ① dislocations and monovacancies are generated upon the application of tensile strain, ② in the presence of hydrogen, monovacancies and hydrogen form complexes, ③ by room temperature annealing, hydrogen is desorbed and the leftover monovacancies from vacancy clusters upon tensile straining.

4. Conclusions

In the present study, the generation process of hydrogen-related defects in austenitic stainless steel SUS 304 was investigated to shed light on the mechanism of the still unresolved important issue of hydrogen embrittlement. The non-destructive and highly sensitive positron annihilation lifetime spectroscopy was used to determine the defect size and concentration. Using this technique, *in-situ* analysis of the defect formation behaviour at the boundary between the elastic region and the plastic deformation region during tensile testing was carried out. The measurements revealed the formation of vacancy clusters already at the early stages of the plastic deformation in the hydrogen-charged samples. These defects are believed to originate from the agglomeration of the vacancies leftover by the vacancy-hydrogen complexes after hydrogen desorption at room temperature and application of tensile strain. Upon application of further tensile straining, the vacancy clusters then become the trigger of the brittle fracture.

Acknowledgement

This research was supported by a research grant from the JFE 21st Century Foundation.

References

1. Barrera O, Bombac D, Chen Y, et al (2018) Understanding and mitigating hydrogen embrittlement of steels: a review of experimental, modelling and design progress from atomistic to continuum. J Mater Sci 53:6251–6290.
2. 南雲道彦 (2008) 水素脆性の基礎—水素の振るまいと脆化機構. 内田老鶴圃
3. Fukai Y (2011) Some Consequences of Hydrogen-induced Superabundant Vacancy Formation in Metals (I). Formation of Hydrogen-induced Vacancies. Materia 50:465–472
4. Chiari L, Fujinami M (2019) Positron Annihilation. In: Ida N, Norbert M (eds) Handbook of Advanced Non-Destructive Evaluation. Springer International Publishing, Cham, pp 1–46
5. Hosoya Y, Inoue A, Masumoto T (1978) Effect of Hydrogen on Crack Propagation Behavior and Microstructures around Cracks in Austenitic Stainless Steels. Tetsu-to-Hagane 64:769–778. https://doi.org/10.2355/tetsutohagane1955.64.6_769
6. Nagumo M (2010) Hydrogen Embrittlement of Austenitic Stainless Steels. J High Press Inst Japan 48:154–165.
7. Ohkubo H, Tang Z, Nagai Y, et al (2003) Positron annihilation study of vacancy-type defects in high-speed deformed Ni, Cu and Fe. Mater Sci Eng A 350:95–101. https://doi.org/10.1016/S0921-5093(02)00705-0